ARTICLE IN PRESS

Applied Energy xxx (2016) xxx–xxx

Contents lists available at ScienceDirect

Applied Energy

journal homepage: www.elsevier.com/locate/apenergy

Dynamic economic dispatch of a hybrid energy microgrid considering building based virtual energy storage system

Xiaolong Jin [a], Yunfei Mu [a,*], Hongjie Jia [a], Jianzhong Wu [b], Tao Jiang [c], Xiaodan Yu [a]

[a] Key Laboratory of Smart Grid of Ministry of Education, Tianjin University, Tianjin 30072, China
[b] Institute of Energy, School of Engineering, Cardiff University, Cardiff CF24 3AA, UK
[c] School of Electrical Engineering, Northeast Dianli University, Jilin, China

HIGHLIGHTS

- A building based virtual energy storage system (VESS) model was developed.
- A dynamic economic dispatch model integrated with VESS was developed.
- The charging/discharging characteristics of the VESS were analyzed.
- The VESS was dispatched within the customer temperature comfort range.

ARTICLE INFO

Article history:
Received 4 April 2016
Received in revised form 15 July 2016
Accepted 16 July 2016
Available online xxxx

Keywords:
Hybrid Energy Microgrid (H-Microgrid)
Virtual energy storage system (VESS)
Dynamic economic dispatch (DED)
Low-carbon building

ABSTRACT

The increasing complexities of hybrid energy Microgrid (H-Microgrid) integrated with renewable generations, dispatchable distribution generators (DGs) and low-carbon buildings require more intelligent dispatch method. The building sector occupies the main body of the energy consumption, which represents a major potential contributor for reducing the daily operating cost of the H-Microgrid. In this paper, a building based virtual energy storage system (VESS) model was developed by utilizing the heat storage capability of the building. Then, a dynamic economic dispatch (DED) model of the H-Microgrid considering the VESS was developed. Finally, the VESS was integrated into the DED model of the H-Microgrid for daily operating cost reduction. The indoor temperature of the building was adjusted within the customer temperature comfort range to manage the charging/discharging power of the VESS. Numerical studies demonstrate that the proposed DED method can make full use of the available capacity of VESS to reduce the daily operating cost, and guarantee the customer temperature comfort level at the same time.

1. Introduction

With the growing concerns over the energy depletion and environmental issues around the world, increasing attention is being paid to technologies in renewable generation utilization and energy efficiency improvement [1]. According to the U.S. Department of Energy, about 40% of total energy is consumed in buildings in industrialized countries, among which 68% is electricity [2]. As a result, a number of countries have taken specific initiatives to encourage a high penetration of renewables and low energy consumption in their building sectors [2–9]. The European Directive (2010/31/EU) shows that all the new buildings in Europe are required to be nearly zero energy buildings by 2020, targeting a high penetration of renewables and low energy consumption [4]. In China, the building sector currently accounts for 27.6% of the total energy use and is estimated to reach 35% by 2020 [5,6]. The Chinese government has paid particular attention to the retrofits and renovations of the existing buildings, and provided financial support for the energy management in large commercial and public buildings [5,7]. The Building Energy Efficiency consortium in the U.S.-China Clean Energy Research Center (CERC) seeks to address research on building operation economic saving technologies and practices [8,9].

As an effective way to handle the uncertainties of the renewable energies, the H-Microgrid provides an economical energy supply for the buildings [10,11]. The increasing complexities of H-Microgrid integrated with renewable generations, dispatchable distribution generators (DGs) and low-carbon buildings [12] require more intelligent dispatch method. It has been shown that 20–30% of the

* Corresponding author.
E-mail addresses: xljin@tju.edu.cn (X. Jin), yunfeimu@tju.edu.cn (Y. Mu), hjjia@tju.edu.cn (H. Jia), wuj5@cardiff.ac.uk (J. Wu), eetaojiang@gmail.com (T. Jiang), yuxd@tju.edu.cn (X. Yu).

http://dx.doi.org/10.1016/j.apenergy.2016.07.080
0306-2619/

Please cite this article in press as: Jin X et al. Dynamic economic dispatch of a hybrid energy microgrid considering building based virtual energy storage system. Appl Energy (2016), http://dx.doi.org/10.1016/j.apenergy.2016.07.080

Nomenclature

Abbreviations

DED	dynamic economic dispatch
VESS	virtual energy storage system
DG	distribution generator
DE	diesel engine
FC	fuel cell
EC	electric chiller
BESS	battery energy storage system

Sets and indices

J, j	set of indexes of the wall orientations of a building
T, t	set of indexes of the dispatch time periods
DG, i	set of indexes of the dispatchable DGs
EC, n	set of indexes of the electric chillers

Parameters and constants

C_{ph}, C_{se}	real-time electricity purchasing/selling prices ($/MW h)
C_{gas}	natural gas price ($/MW h)
P_{el}	electric load of the H-Microgrid (kW)
P_{PV}, P_{WT}	electric power generated by photovoltaic/wind turbine (kW)
U_{wall}, U_{win}	heat transfer coefficient of the wall/window in the building [W/(m^2·K)]
$F_{wall,j}$	the area of the total wall surface at the j-wall orientation (m^2)
$F_{win,j}$	the area of the total window surface at the j-wall orientation (m^2)
T_{out}, T_{in}	outdoor/indoor temperature (°C)
T_{set}	indoor temperature set-point (°C)
τ_{win}, SC	the glass transmission coefficient and shading coefficient of the windows
α_w	absorbance coefficient of the wall external surface
$\dot{Q}_{in}$	internal heat gains from people, appliances and lighting (kW)
ρ, C, V	the density (kg/m^3), specific heat capacity [J/(kg·°C)] and volume of the air (m^3) in the building
a, b, c	fuel cost coefficients of the diesel engine
η_{FC}	efficiency of the fuel cell
EER_{EC}	energy efficiency ratio of the electric chiller
η_{ch}, η_{dis}	charging/discharging efficiency of the BESS
CAP_{bt}	the rated capacity of the BESS (kW h)
SOC, δ	the state of charge/self-discharge ratio of the BESS
E_{bt}	the residual energy of the BESS (kW h)
ρ_{DG}, ρ_{su}	maintenance cost ($/kW h) and startup cost ($) of a dispatchable DG
R_u, R_d	ramp-up/ramp-down rate of a dispatchable DG (kW/min)
S_u, S_d	startup/shutdown rate of a dispatchable DG (kW/min)
UT, DT	minimum up/down time periods of a dispatchable DG (h)
ρ_{WT}, ρ_{PV}	maintenance cost of the WT and the PV ($/kW h)
ρ_{bt}, ρ_{EC}	maintenance cost of the BESS and the electric chiller ($/kW h)

Variables

P_{ex}	electric power exchange with the external grid (kW)
P_{gas}	natural gas purchase (kW)
P_{DE}, P_{FC}	electric power generated by DE/FC (kW)
P_{bt}	charging/discharging power of the BESS (kW)
$\dot{Q}_{EC}$	cooling power generated by the electric chiller (kW)
$\dot{Q}_{cl,building}$	cooling load of the building with VESS (kW)
$\dot{Q}'_{cl,building}$	cooling load of the building without VESS (kW).
P_{DG}	power generation of a dispatchable DG (kW)
U_{DG}	operation status of a dispatchable DG
U'_{DG}, U''_{DG}	startup/shutdown status of a dispatchable DG
T^{on}, T^{off}	number of successive ON/OFF time periods of a dispatchable DG (h)

energy consumption of the building sector, which occupies the main body of the energy consumption of the H-Microgrid, can be saved through economic dispatch without changing the structure and hardware configuration of the H-Microgrid [2].

Several studies have been carried out to investigate the economic dispatch for the H-Microgrid. An economic dispatch model was developed in [2] for a low-carbon building to minimize the total cost of electricity and natural gas. A hierarchical energy management system was proposed in [10] for the H-Microgrid based on an energy hub model. A model predictive control based strategy using nonlinear programming model was proposed to dispatch a building Microgrid under dynamic electricity price [12]. The mixed-integer nonlinear programming model was proposed to solve the economic dispatch problem for a building Microgrid and handle the discrete working ranges of the energy systems [13]. A multi-objective mixed-integer linear programming model was proposed to reduce the daily operating cost and the total emission of the H-Microgrid [14].

The controllable loads of the H-Microgrid, such as the refrigerators, freezers, air conditioners, water heaters, heat pumps and electric vehicles (EVs), *etc.*, can change their normal power consumption patterns to participate in the economic dispatch of the H-Microgrid due to their energy storage and controllable characteristics [15–21]. The charging strategy of the EVs in an office building Microgrid equipped with a photovoltaic (PV) system and a combined heat and power unit was discussed in [18]. In [19], a heuristic operation strategy for a commercial building Microgrid containing EVs and a PV system was proposed to improve the self-consumption capability of PV energy. An economic dispatch model is proposed for a residential Microgrid including a charging spot with a Vehicle-to-Grid system and renewable energy sources to reduce the daily operating cost [20]. A multi-objective dispatch model is proposed for a Microgrid containing EVs, responsive loads and renewable generations to reduce the daily operating cost and the total emission [21].

The existing research works have made good contributions to the economic dispatch of H-Microgrid. However, the coupling relationship among the heating/cooling demand of a building, the customer temperature comfort range and the outdoor temperature are not well considered in the economic dispatch of the H-Microgrid. Actually, the heating/cooling demand of a building can be adjusted in the economic dispatch process to reduce daily operating cost without disturbing the temperature comfort level of the building. For this purpose, the mathematical relationship among the indoor temperature, cooling demand and outdoor temperature is established in this paper based on the building thermal equilibrium equation. Then, a building based virtual energy storage system (VESS) model was developed as a dispatchable unit to participate in the economic dispatch of the H-Microgrid for daily operating cost reduction.

On the other hand, the economic dispatch of H-Microgrid can be divided into static economic dispatch and dynamic economic dispatch (DED) [22–24]. Compared with static economic dispatch, the DED is better suited to the requirements of a H-Microgrid in actual operation because it not only considers the minimization daily operating cost in a dispatch cycle but also satisfies energy loads, ramp limits and other constraints in every time interval [24]. Therefore, a DED model integrated with VESS was developed for the H-Microgrid in this paper. The charging/discharging power of the VESS was dispatched within the customer temperature comfort range to reduce the daily operating cost. The main contributions of this paper are summarized as follows:

(1) The mathematical relationship among the indoor temperature, cooling demand and outdoor temperature is established based on the building thermal equilibrium equation. Then, a building based VESS model is built.
(2) The VESS model is integrated into a DED model to dispatch all the energy systems and the VESS for daily operating cost reduction. The indoor temperature of the building is adjusted within the customer temperature comfort range to manage the charging/discharging power of the VESS.
(3) The charging/discharging characteristics between the VESS and battery energy storage system (BESS) were compared. The relationship between the charging/discharging characteristics of the VESS and the electricity prices were analyzed.

2. Models of the virtual energy storage system and DGs in H-Microgrid

A H-Microgrid containing different buildings is shown in Fig. 1. The H-Microgrid is connected to an external grid and integrated with renewable generations, i.e., wind turbine (WT) and PV, dispatchable DGs, i.e., diesel engine (DE) and fuel cell (FC), and other devices, i.e., BESS and electric chillers (ECs). The buildings constitute the energy loads of the H-Microgrid. All the energy systems and building based VESSs are dispatched to satisfy the electric and heating/cooling loads in the H-Microgrid.

2.1. Virtual energy storage system model

The heat storage capability of a building is an important factor to describe the building thermal performance [25]. For a building, the heating/cooling energy can be stored over a short period of time in a building based on its heat storage capability [25]. Therefore, the heating/cooling equipment can be started in advance or increase its energy consumption when the electricity price is low. In the same way, it can be shut down in advance or reduce its energy consumption when the electricity price is high. This is because the heating/cooling demand can be adjusted within the customer temperature comfort range of the building due to the heat storage capability of the building. With this capability, the building is modeled as a VESS to participate in the DED of the H-Microgrid for daily operating cost reduction.

Firstly, the mathematical relationship among the indoor temperature, heating/cooling demand (equals to the heating/cooling power generated by the heating/cooling equipment) and outdoor temperature is established by using the building thermal equilibrium equation shown in Eq. (1) [26].

$$\Delta Q = \rho \times C \times V \times \frac{dT_{in}}{dt} \tag{1}$$

where ΔQ is the rate of change of the indoor air heat energy in a building; dT_{in}/dt is the indoor temperature change per unit time in a building.

Considering a summer cooling scenario, the building is modeled as a single isothermal air volume (shown in Fig. 2) [27]. This volume exchanges heat with the external air through the sum of walls and the sum of windows and receives internal heat gains. The heat contributions due to the solar radiation on the opaque surface of the external walls and transparent surface of the windows are also considered. Then, the Eq. (1) was changed to Eq. (2), in which the following contributions are taken into account:

$$\rho \times C \times V \times \frac{dT_{in}}{dt} = \dot{Q}_{wall} + \dot{Q}_{win} + \dot{Q}_{in} + \dot{Q}_{sw} + \dot{Q}_{sg} - \dot{Q}_{EC} \tag{2}$$

(i) $\dot{Q}_{wall}$ is the heat transfer through the external walls (kW); It is calculated by summing the contribution of each wall of a building, as shown in Eq. (3). The roof of a building was accounted for as part of the external walls [28].
(ii) $\dot{Q}_{win}$ is the heat transfer across the windows (kW); It is calculated by summing the contribution of each window of a building, as shown in Eq. (4).

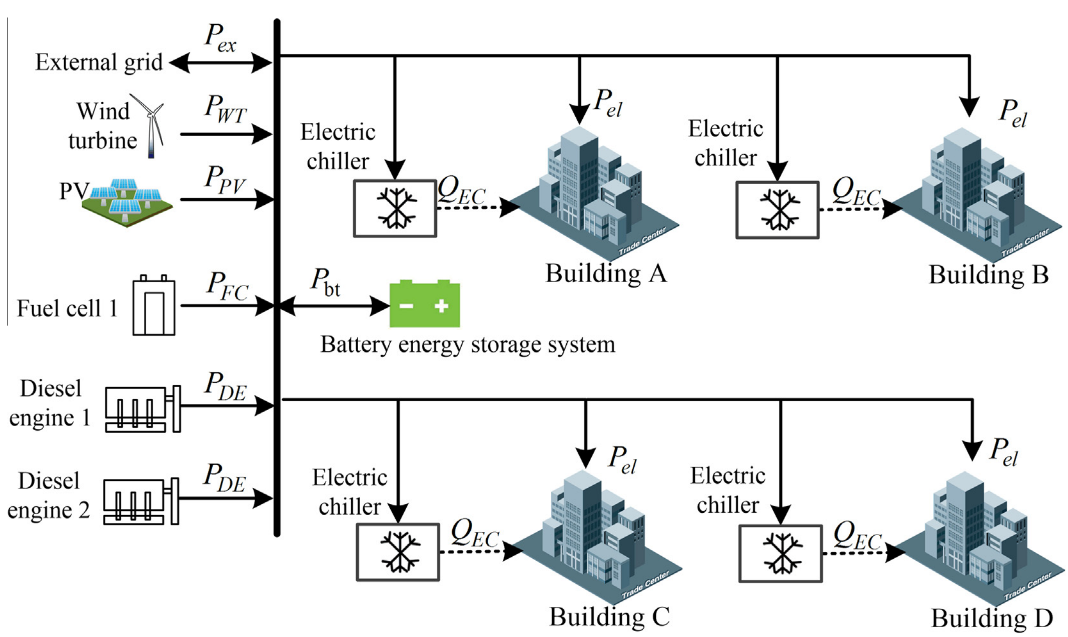

Fig. 1. Schematic diagram of a H-Microgrid containing buildings.

Please cite this article in press as: Jin X et al. Dynamic economic dispatch of a hybrid energy microgrid considering building based virtual energy storage system. Appl Energy (2016), http://dx.doi.org/10.1016/j.apenergy.2016.07.080

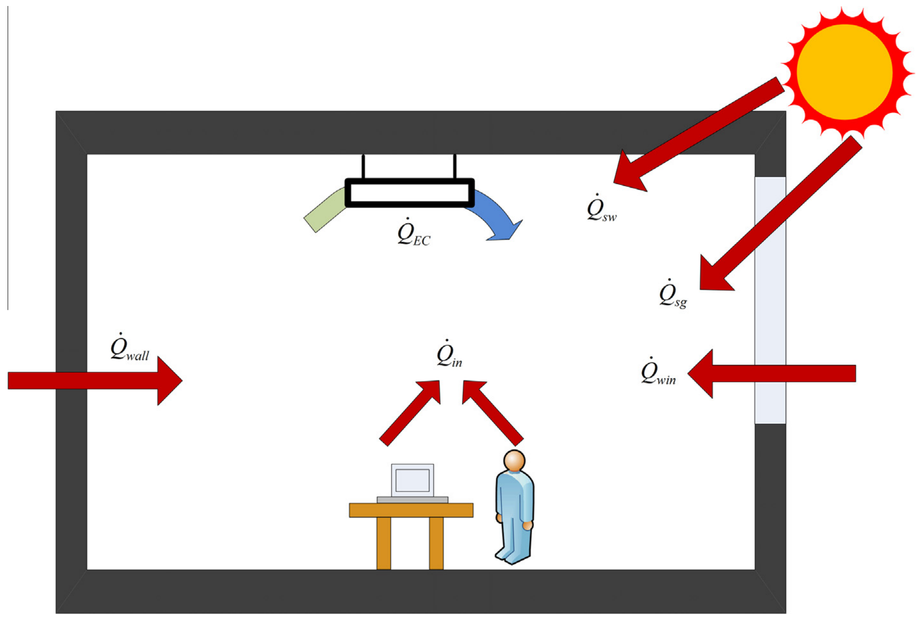

Fig. 2. Schematic of heat transfer of the internal air volume under the summer cooling scenario.

(iii) $\dot{Q}_{in}$ is the internal heat gains (kW).

(iv) $\dot{Q}_{sw}$ is the heat contribution due to the solar radiation on the opaque surface of the external walls (kW); It is calculated by summing the heat contribution due to solar radiation on each external wall (south, west, north and east orientations) according to the ISO 13790 [29], as shown in Eq. (5). Also, the external surface heat resistance for convection and radiation of the external wall j, $R_{se,j}$, is considered in Eq. (5). A typical method to calculate the $R_{se,j}$ is given in [30], which takes both radiation and convection terms into account.

(v) $\dot{Q}_{sg}$ is the whole solar radiation transmitted across the windows (kW); It is calculated according to Eq. (6). It is assumed that the total windows surfaces are distributed in the south, west, north and east orientations of the walls in a building uniformly [31].

(vi) $\dot{Q}_{EC}$ is the cooling power generated by the cooling equipment (kW).

$$\dot{Q}_{wall} = \sum_{j \in J} U_{wall} \times F_{wall,j} \times (T_{out} - T_{in}) \tag{3}$$

$$\dot{Q}_{win} = \sum_{j \in J} U_{win} \times F_{win,j} \times (T_{out} - T_{in}) \tag{4}$$

$$\dot{Q}_{sw} = \sum_{j \in J} \alpha_w \times R_{se,j} \times U_{wall} \times F_{wall,j} \times I_{T,j} \tag{5}$$

$$\dot{Q}_{sg} = \sum_{j \in J} \tau_{win} \times SC \times F_{win,j} \times I_{T,j} \tag{6}$$

where $I_{T,j}$ is the total solar radiation on the walls/windows surface at the j-wall orientation (kW/m^2). In this paper, $I_{T,j}$ is determined according to the method presented in Duffie and Beckman [32], which is a commonly used method to calculate the total solar radiation on a tilted surface [33]. It can be calculated as sum of various types of solar radiation, i.e., beam, diffuse and reflected radiation, given in Duffie and Beckman [32], as shown in Eq. (7).

$$I_T = I_b \times R_b + I_d \times \left(\frac{1+\cos\beta}{2}\right) + I \times \rho_g \times \left(\frac{1-\cos\beta}{2}\right) \tag{7}$$

where I_b, I_d and I represent beam, diffuse and total radiation on horizontal surface respectively (kW/m^2); ρ_g is the ground reflectance and is taken as 0.2 in the present study [33]; R_b is geometric factor which is defined as the ratio of beam radiation on a tilted surface to that on a horizontal surface, which is expressed as:

$$R_b = \frac{\cos\theta}{\cos\theta_z} \tag{8}$$

where θ and θ_z are incidence and zenith angles. Detailed calculation procedures for R_b can be found in [32].

Eq. (2) was developed to express the mathematical relationship among the indoor temperature, heating/cooling power demand and outdoor temperature. As shown in Eq. (2), when the indoor temperature is increased, i.e., $dT_{in} > 0$, the indoor air heat energy is increased, i.e., $(\dot{Q}_{wall} + \dot{Q}_{win} + \dot{Q}_{in} + \dot{Q}_{sw} + \dot{Q}_{sg} - \dot{Q}_{EC}) \times dt > 0$, which means that energy is stored during dt. On the other hand, when the indoor temperature is decreased, i.e., $dT_{in} < 0$, the indoor air heat energy is decreased, i.e., $(\dot{Q}_{wall} + \dot{Q}_{win} + \dot{Q}_{in} + \dot{Q}_{sw} + \dot{Q}_{sg} - \dot{Q}_{EC}) \times dt < 0$, which means that energy is discharged during dt. Then, due to the heat storage capability of a building, the cooling demand (equals to the cooling power generated by the electric chiller) and indoor temperature are adjusted to respond to DED of H-Microgrid and the VESS is modeled (shown in Fig. 2). Then, the charging/discharging power of the building based VESS, as shown in Eq. (9), is obtained following Eq. (2).

The principle of the VESS is that the cooling energy generated by the electric chiller during dt ($\dot{Q}_{EC}$) can be stored in the building when the electricity price is low, i.e., the electric chiller can be started in advance or increase its energy consumption during dt (the VESS is charged, $\dot{Q}_{VESS,t} < 0$). In the same way, $\dot{Q}_{EC}$ can be discharged in the building when the electricity price is high during dt, i.e., the electric chiller can be shut down in advance or reduce its energy consumption during dt (the VESS is discharged, $\dot{Q}_{VESS,t} > 0$). The indoor temperature comfort range and temperature set-point are considered in the DED model to guarantee the customer comfort level.

$$\dot{Q}_{VESS,t} = \dot{Q}'_{cl,building,t} - \dot{Q}_{cl,building,t} \tag{9}$$

2.2. The mathematical model of DGs

(1) Diesel engine

For DE, the fuel cost depends on the power generation and fuel cost coefficients, which is shown in Eq. (10).

$$f_{fuel}(P_{DE,t}) = aP_{DE,t}^2 + bP_{DE,t} + c \tag{10}$$

(2) Fuel cell

For FC, the fuel cost depends on the power generation and efficiency η_{FC}, which is shown in Eq. (11).

$$f_{fuel}(P_{FC,t}) = C_{gas} \times P_{gas} = C_{gas} \times (P_{FC,t}\Delta t/\eta_{FC}) \tag{11}$$

(3) Electric chiller

The electricity consumption of the EC is determined by the cooling demand and the coefficient of performance, as shown in Eq. (12).

$$\dot{Q}_{EC,t} = P_{EC,t} \times EER_{EC} \tag{12}$$

(4) BESS

The state of charge (SOC) of the BESS refers to the ratio of the residual energy to the rated energy. The SOC at dispatch time interval t is described in Eq. (13).

$$SOC_t = \begin{cases} SOC_{t-1}(1-\delta) - P_{bt,t}\Delta t\eta_{ch}/CAP_{bt} & P_{bt,t} \leqslant 0 \\ SOC_{t-1}(1-\delta) - P_{bt,t}\Delta t/(\eta_{dis}CAP_{bt}) & P_{bt,t} > 0 \end{cases} \tag{13}$$

3. Formulation of the DED model of the H-Microgrid

3.1. Objective function

The objective function depicted in Eq. (14) is to minimize the total daily operating cost for the H-Microgrid.

$$\begin{aligned} \min \sum_{t\in T}\Bigg\{ & \left(\tfrac{C_{ph,t}+C_{se,t}}{2}P_{ex,t} + \tfrac{C_{ph,t}-C_{se,t}}{2}|P_{ex,t}|\right) \\ & + \left(\sum_{i\in DG}[f_{fuel}(P_{DG,i,t}) + \rho_{DG,i} \times P_{DG,i,t} + \rho_{su,i} \times U'_{DG,i,t}]\right) \\ & + \left(\rho_{WT}P_{WT,t} + \rho_{PV}P_{PV,t} + \rho_{bt}|P_{bt,t}| + \sum_{n\in EC}\rho_{EC}P_{EC,n,t}\right)\Bigg\} \end{aligned} \tag{14}$$

The first term in Eq. (14) represents the cost for electricity purchase from the external grid; The second term represents the fuel costs depicted by fuel cost function $f_{fuel}(\cdot)$, maintenance costs and the startup costs of all the dispatchable DGs; the third term is the maintenance costs of other devices of the H-Microgrid.

3.2. Constraints

(1) Electrical power balance:

$$\begin{aligned} & \sum_{i\in DG}P_{DG,i,t} + P_{ex,t} + P_{WT,t} + P_{PV,t} + P_{bt,t} \\ & = P_{el,t} + \sum_{n\in EC}P_{EC,n,t}, \quad \forall i \in DG,\ \forall n \in EC,\ \forall t \in T \end{aligned} \tag{15}$$

(2) Cooling demand balance:

$$\dot{Q}_{EC,t} = \dot{Q}_{cl,building,t}, \quad \forall t \in T \tag{16}$$

(3) Building thermal equilibrium equation:

Due to the transient effect and the thermal capacity of the building mass, the heat flow of the building envelopes developed in Eq. (2) is presented as unsteady heat flow [33]. In order to solve the DED model of the H-Microgrid considering the unsteady heat flow of the building envelopes, the differential equation, as shown in Eq. (2), is converted to a finite difference equation with a forward difference approximation on the time derivative [33]. The finite difference equation is considered as a constraint of the DED model, as shown in Eq. (17).

$$\begin{aligned} \Delta t\Bigg[& \sum_{j\in J}U_{wall} \times F_{wall,j} \times (T_{out,t} - T_{in,t}) + \sum_{j\in J}U_{win} \times F_{win,j} \times (T_{out,t} - T_{in,t}) \\ & + \sum_{j\in J}\alpha_w \times R_{se,j} \times U_{wall} \times F_{wall,j} \times I_{T,j,t} + \sum_{j\in J}\tau_{win} \times SC \times F_{win,j} \\ & \times I_{T,j,t} + \dot{Q}_{in,t} - \dot{Q}_{EC,t}\Bigg] - \rho CV(T_{in,t+1} - T_{in,t}) = 0, \quad \forall t \in T \end{aligned} \tag{17}$$

(4) Technical constraints from the dispatchable DGs:

For each dispatchable DG, the power generation is constrained by the upper and lower power output limits. The power generations between two successive dispatch time intervals are constrained by ramp-up (ramp-down) rates as well as startup (shutdown) rates. In the DED model, the constraints from the dispatchable DGs are introduced to consider the inherent link among the dispatch time intervals.

$$\underline{P}_{DG,i,t}U_{DG,i,t} \leqslant P_{DG,i,t} \leqslant \overline{P}_{DG,i,t}U_{DG,i,t}, \quad \forall i \in DG,\ \forall t \in T \tag{18}$$

$$P_{DG,i,t} - P_{DG,i,t-1} \leqslant R_{u,i}\Delta tU_{DG,i,t-1} + S_{u,i}\Delta tU'_{DG,i,t}, \quad \forall i \in DG,\ \forall t \in T \tag{19}$$

$$P_{DG,i,t-1} - P_{DG,i,t} \leqslant R_{d,i}\Delta tU_{DG,i,t} + S_{d,i}\Delta tU''_{DG,i,t}, \quad \forall i \in DG,\ \forall t \in T \tag{20}$$

$$U'_{DG,i,t} = \max(0, U_{DG,i,t} - U_{DG,i,t-1}), \quad \forall i \in DG,\ \forall t \in T \tag{21}$$

$$U''_{DG,i,t} = \max(0, U_{DG,i,t-1} - U_{DG,i,t}), \quad \forall i \in DG,\ \forall t \in T \tag{22}$$

where $U_{DG,i,t}$, $U'_{DG,i,t}$ and $U''_{DG,i,t}$ are the operation status ("1" represents 'ON'-state while "0" represents 'OFF'-state); the startup status ("1" for startup, "0" otherwise) and the shutdown status ("1" for shutdown, "0″ otherwise) of dispatchable DG i at time interval t; $\underline{P}_{DG,i,t}$ and $\overline{P}_{DG,i,t}$ are the lower and upper power output limits of dispatchable DG i at time interval t.

The dispatchable DGs are also constrained by the minimum up and down time limits shown in Eqs. (23) and (24).

$$T_{i,t}^{on} \geqslant UT_i(U_{DG,i,t} - U_{DG,i,t-1}), \quad \forall i \in DG,\ \forall t \in T \tag{23}$$

$$T_{i,t}^{off} \geqslant DT_i(U_{DG,i,t-1} - U_{DG,i,t}), \quad \forall i \in DG,\ \forall t \in T \tag{24}$$

(5) Technical constraints from the electric chiller:

The constraint for the cooling output of electric chiller is shown in Eq. (25).

$$0 \leqslant Q_{EC,t} \leqslant \overline{Q}_{EC}, \quad \forall t \in T \tag{25}$$

where $\overline{Q}_{EC}$ is the upper cooling power output limit of the electric chiller.

(6) Technical constraints from BESS:

For the BESS, the charging/discharging power and the SOC are constrained by the upper and lower limits shown in Eqs. (26) and (27); For the energy balance, the stored energy inside the BESS is set the same as the initial stored energy, as shown in Eq. (29).

$$\underline{P}_{bt} \leqslant P_{bt,t} \leqslant \overline{P}_{bt}, \quad \forall t \in T \tag{26}$$

$$\underline{SOC} \leqslant SOC_t \leqslant \overline{SOC}, \quad \forall t \in T \tag{27}$$

$$SOC_t = \frac{E_{bt,t}}{CAP_{bt}} \tag{28}$$

$$\sum_{t\in T}P_{bt,t} = 0 \tag{29}$$

Please cite this article in press as: Jin X et al. Dynamic economic dispatch of a hybrid energy microgrid considering building based virtual energy storage system. Appl Energy (2016), http://dx.doi.org/10.1016/j.apenergy.2016.07.080

where $\underline{P}_{bt}$ and $\overline{P}_{bt}$ are the lower and upper charging/discharging power limits of the BESS; $\underline{SOC}$ and $\overline{SOC}$ are the lower and upper SOC limits of the BESS.

(7) Indoor temperature constraint:

$$\underline{T_{in}} < T_{in,t} < \overline{T_{in}}, \quad \forall t \in T \tag{30}$$

where $\underline{T_{in}}$ and $\overline{T_{in}}$ are the lower and upper indoor temperature limits of a building.

(8) Electric power purchase constraint:

$$\underline{P_{ex}} < P_{ex,t} < \overline{P_{ex}}, \quad \forall t \in T \tag{31}$$

where $\underline{P_{ex}}$ and $\overline{P_{ex}}$ are the lower and upper electric power purchase limits. The DED model was implemented using IBM ILGO CPLEX under MATLAB platform [34–36].

4. Case studies

4.1. Case study

A H-Microgrid shown in Fig. 1 containing different buildings was used to verify the effectiveness of the developed DED method. Four different buildings are investigated. In particular, the considered buildings vary from residential one to commercial one by changing the parameters of heat transfer coefficient of wall, heat transfer coefficient of window, window to wall ratio and the occupied hours. All the buildings are represented by a parallelepiped with a squared floor. The parameters of the buildings are given in Table 1 [26,27,37–39].

- Building A (Residential building): The occupied hours are set to be from 00:00 a.m. to 9:00 a.m. and from 18:00 p.m. to 23:00 p.m.
- Building B (Office building): The occupied hours are set to be from 8:00 a.m. to 20:00 p.m.
- Building C (Apartment building): The occupied hours are set to be the whole day.
- Building D (Mall building): The occupied hours are set to be from 10:00 a.m. to 22:00 p.m.

The values of the parameters air mass density ρ and air specific heat ratio C are set to be 1.2 kg/m^3 and 1000 J/(kg·°C) respectively. The forecasted outdoor temperature in a typical summer day are shown in Fig. 3. The forecasted solar radiation on horizontal surface [40] and calculated incident solar radiation on the walls/windows surface at south, west, north and east orientations [32] are shown in Fig. 4. The forecasted renewable generations and forecasted electric loads with internal heat gains of the four buildings in a typical summer day are shown in Figs. 5 and 6 respectively. Note that, the internal heat gains of the four buildings (shown in Fig. 6) are presented as the sum of internal heat gains from people, appliances and lighting [41,42]. All the forecasted data are typical daily profiles, which are used as forecasted input data for DED of H-Microgrid. The indoor temperature comfort range is set to be from 20 °C to 25 °C during occupied hours. The indoor temperature set-point is set to be 22.5 °C [43]. The electric chillers are switched on during occupied hours [44]. The proposed DED method dispatches the H-Microgrid over a 24-h time-period (T = 24 h) with 15-min interval.

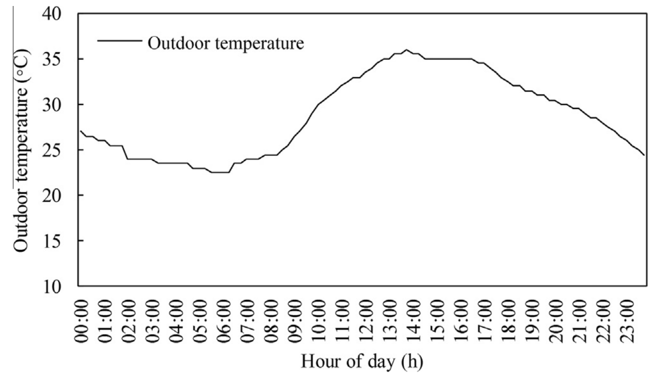

Fig. 3. Forecasted outdoor temperature.

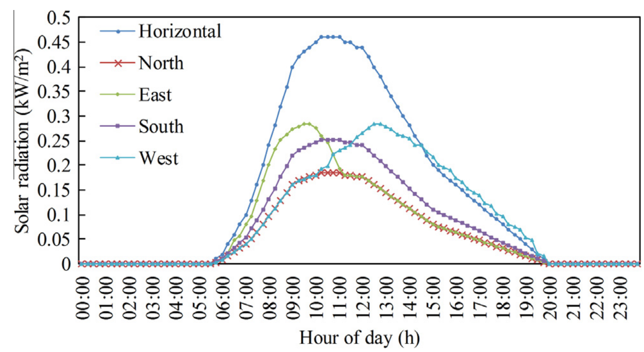

Fig. 4. Values of incident solar radiation flux.

The real-time electricity prices from NYISO are used in this paper [45], as shown in Fig. 7. The price for selling electricity back to the external grid is set to be 0.8 times the price for purchasing electricity. The natural gas price is 42.5$/MW h [11]. The technical/economic parameters of the dispatchable DGs and the parameters of the other devices are shown in Tables 2–4 with the data collecting from [46–52]. The fuel cost coefficients of the DE are set to be a = 44 ($/h/MW^2), b = 65.34 ($/h/MW) and c = 1.1825 ($/h).

4.2. Dynamic economic dispatch results analysis

Two comparative cases are presented as follows:

Case (1): Dispatch the H-Microgrid without VESSs and keep the indoor temperatures of the buildings at the desired set points.
Case (2): Dispatch the H-Microgrid with VESSs. The cooling demands and indoor temperatures of the buildings are adjusted within the customer temperature comfort ranges.

The dispatch results of the electricity generation/consumption of the H-Microgrid for Case 1 and Case 2 are shown in Fig. 8. For

Table 1
Building parameters.

Building	U_{wall} [W/(m^2·K)]	F_{wall} (m^2)	U_{win} [W/(m^2·K)]	Window to wall ratio (%)	Long side (m)	Short side (m)	Height (m)
Building A	1.092	1000	2.800	45	30	20	9
Building B	0.908	2400	2.750	75	40	20	30
Building C	1.146	1500	2.800	60	30	20	20
Building D	0.820	2700	2.500	65	50	30	20

Please cite this article in press as: Jin X et al. Dynamic economic dispatch of a hybrid energy microgrid considering building based virtual energy storage system. Appl Energy (2016), http://dx.doi.org/10.1016/j.apenergy.2016.07.080

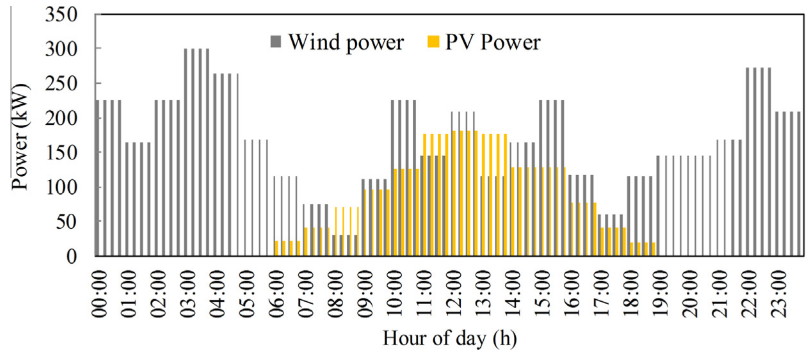

Fig. 5. Forecasted typical daily renewable generation profiles.

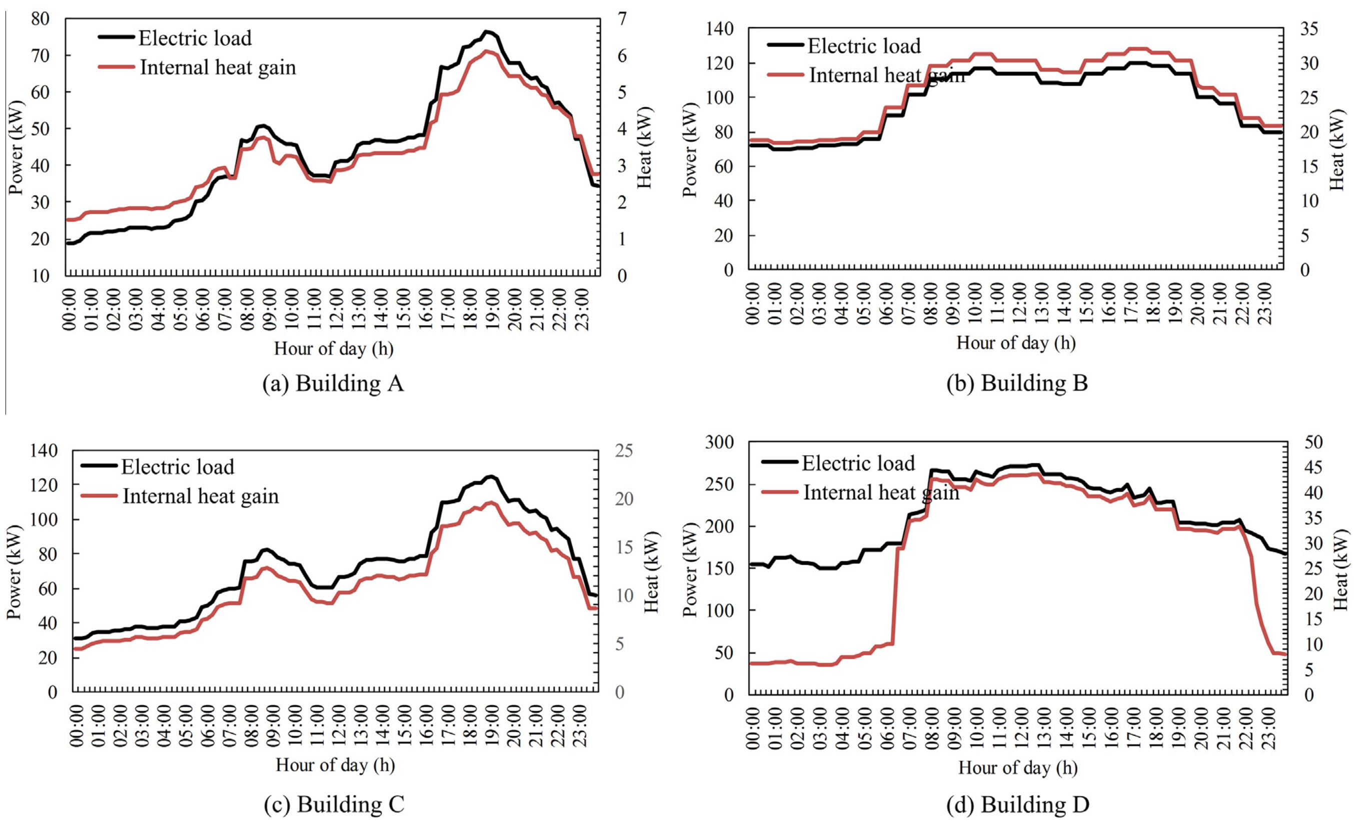

Fig. 6. Forecasted electric loads and internal heat gains of the four buildings.

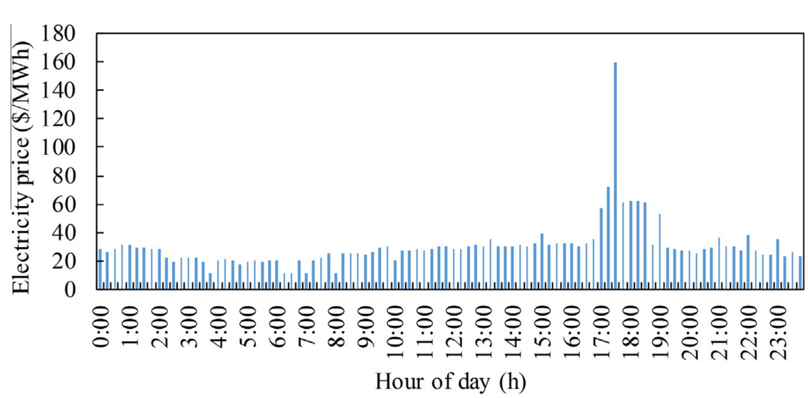

Fig. 7. Real time price.

Table 2
Technical parameters of the dispatchable DGs.

DG type	$\underline{P}_{DG}$(kW)	$\overline{P}_{DG}$ (kW)	R_u (kW/min)	R_d (kW/min)	S_u (kW/min)	S_d (kW/min)	UT(h)	DT (h)	Number of DGs
DE	20	100	2	2	2	2	2	1	2
FC	12	120	2	2	2	2	2	1	1

Table 3
Economic parameters of the dispatchable DGs.

Type	DE	FC	EC	WT	PV	BESS
Startup cost ($)	0.24	0.32	–	–	–	–
Maintenance cost ($/kW h)	0.0033	0.0046	0.001	0.001	0.001	0.001

Table 4
Parameters of the other devices.

Parameters	Value
EER_{EC}	4
$\overline{P}_{EC,1}/\underline{P}_{EC,1}$	120 kW/0 kW
$\overline{P}_{EC,2}/\underline{P}_{EC,2}$	200 kW/0 kW
$\overline{P}_{EC,3}/\underline{P}_{EC,3}$	120 kW/0 kW
$\overline{P}_{EC,4}/\underline{P}_{EC,4}$	600 kW/0 kW
$\overline{P_{ex}}/\underline{P_{ex}}$	600 kW/−600 kW
CAP_{bt}	400 kW h
$\overline{SOC}/\underline{SOC}$	0.8/0.2
$\overline{P}_{bt}/\underline{P}_{bt}$	40 kW/−40 kW
η_{ch}/η_{dis}	0.95/0.95
δ	0.04
η_{FC}	0.55

the time periods from 17:00 to 19:00, as the electricity purchase prices are higher than that of other periods, the H-Microgrid tends to purchase less electric power from the external grid and dispatch more power generated by dispatchable DGs in both Case 1 and Case 2. In contrast, for the time periods including 0:00–16:00 and 20:00–23:00, as the electricity purchase prices are lower than that of other periods, the H-Microgrid tends to purchase more electric power from the external grid and reduce power generation from the dispatchable DGs for cost savings in both Case 1 and Case 2. The daily operating cost in Case 1 is $402.9, while the daily operating cost in Case 2 is $387.4. The daily operating cost can be reduced by 3.85% in Case 2.

The dispatch results of all the dispatchable DGs for Case 1 and Case 2 are shown in Fig. 9. It can be observed from Fig. 9, all the dispatchable DGs are dispatched satisfying the technical constraints, as shown in Eqs. (18) and (24). All the dispatchable DGs are committed and dispatched at their maximum capacities during high electricity purchase price periods (17:00–19:00) and switched off or reduced power generation for cost savings during low electricity purchase price periods (0:00–16:00 and 20:00–23:00). However, due to electric power purchase constraint, as shown in Eq. (31), the required electric power cannot be imported from the external grid in both Case 1 and Case 2 at 10:00, as shown in

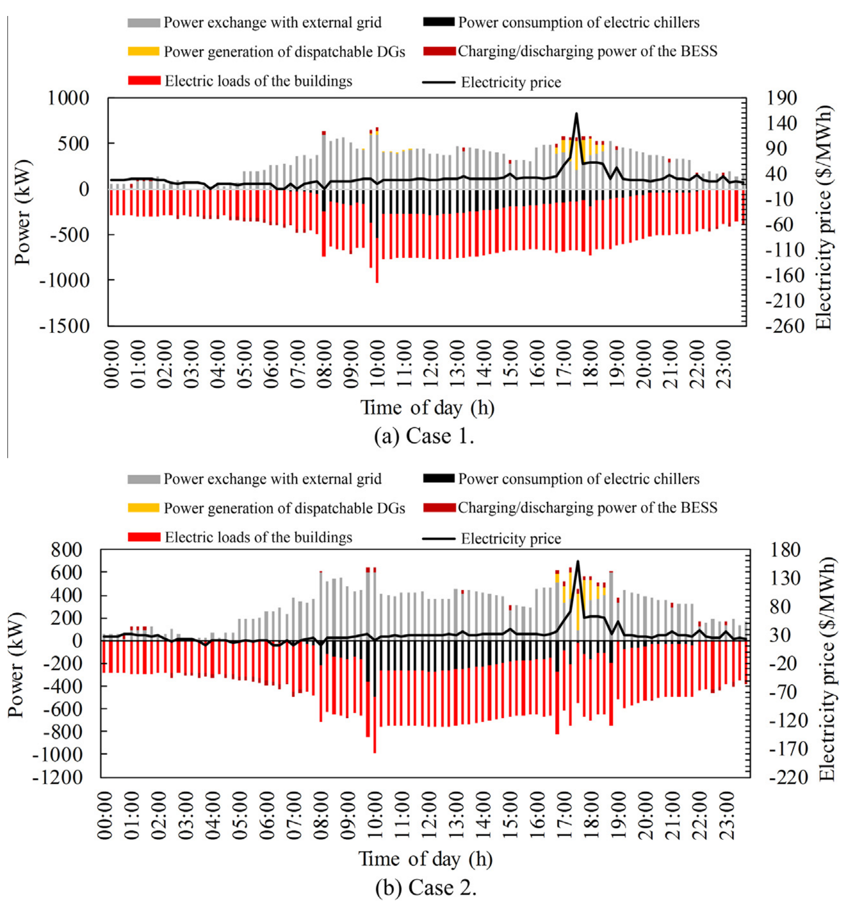

Fig. 8. Dispatch results of the electricity generation/consumption in a typical day.

Please cite this article in press as: Jin X et al. Dynamic economic dispatch of a hybrid energy microgrid considering building based virtual energy storage system. Appl Energy (2016), http://dx.doi.org/10.1016/j.apenergy.2016.07.080

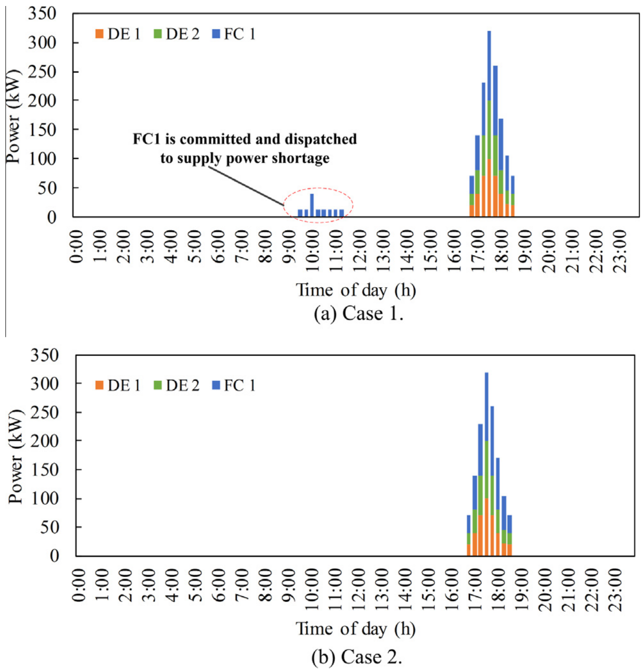

Fig. 9. Dispatch results of the dispatchable DGs in a typical day.

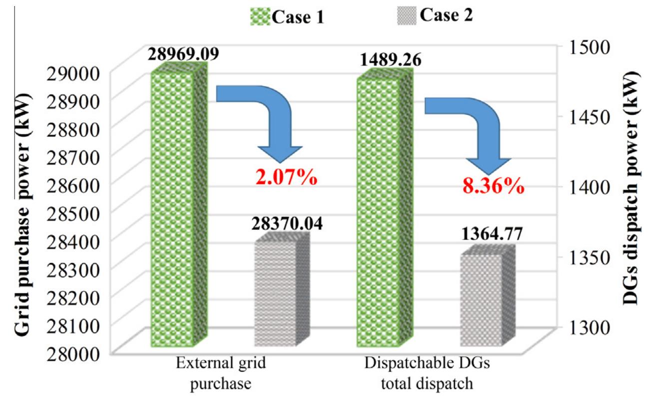

Fig. 11. Overall power purchased from the external grid and dispatched by the dispatchable DGs.

Fig. 10. Therefore, the FC is committed and dispatched at 10:00 to generate power to supply the electric power shortage in Case 1. Compared with Case 1, the cooling demands of the buildings in Case 2 are adjusted to reduce the power consumptions of the electric chillers, which has resulted in no power shortage at 10:00. Therefore, no dispatchable DG is committed and dispatched at 10:00 and more cost savings are achieved in Case 2. It is worth noting that only FC is committed and dispatched to supply the power shortage at 10:00 in Case 1. This is because the FC has low cost coefficients compared with the DEs.

Compared with Case 1, the advantages of Case 2 lie in three aspects:

(1) By introducing VESSs to the H-Microgrid DED process, the cooling demands and indoor temperatures can be adjusted within the customer temperature comfort ranges to reduce the daily operating cost (decrease from \$402.9 to \$387.4).
(2) The total startup and shutdown times of the dispatchable DGs are decreased in Case 2. This will reduce the startup costs of dispatchable DGs and furthermore extend the service life of them.
(3) More free capacity of the dispatchable DGs can be obtained in Case 2. Fig. 11 depicts the overall power purchased from the external grid and dispatched by the dispatchable DGs. It can be observed that introducing the VESSs into the H-Microgrid DED process not only decreases the total external grid power purchase, but also brings about a more 8.36% free capacity for DGs.

The dispatch results of the VESSs, the cooling demand of the building with ($\dot{Q}_{cl,building,t}$) and without ($\dot{Q}'_{cl,building,t}$) VESS are shown in Fig. 12. When $\dot{Q}_{cl,building,t}$ is larger than $\dot{Q}'_{cl,building,t}$, the VESS operates in charging mode; when $\dot{Q}_{cl,building,t}$ is smaller than $\dot{Q}'_{cl,building,t}$, the VESS operates in discharging mode. The dispatch results of VESSs show that the VESSs can be charged or discharged according to the actual dispatch demand of the H-Microgrid. The VESSs are dispatched only during the occupied hours (the electric chillers operate in 'ON'-state only during the occupied hours).

The dispatch results also show that the VESSs tend to operate in discharging mode to reduce the daily operating cost. However, due to the indoor temperature constraints and energy dissipation characteristics of the buildings, the VESSs are charged after several time intervals of discharging, as shown in Fig. 12. Generally, the overall quantity of the discharged energy is larger than quantity of the charged energy of a VESS in the whole DED day, which contributes to the economic savings.

Due to the heat storage capability of the buildings, the cooling demands of the buildings can be adjusted according to the time-sensitive electricity prices to reduce the daily operating cost. Therefore, the dispatch results of the building based VESSs and the time-sensitive electricity prices are closely tied. The relation-

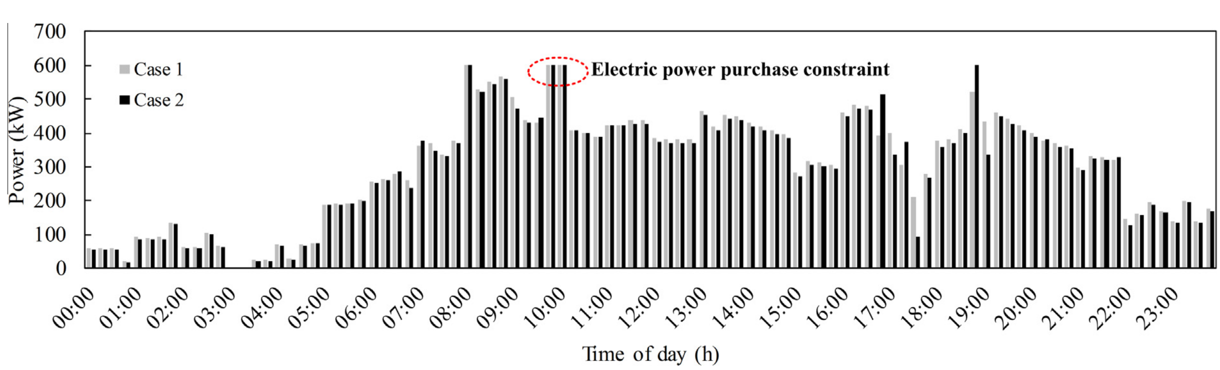

Fig. 10. Electric power purchase in a typical day.

ship between dispatch results of VESSs and electricity prices is shown in Fig. 13. The VESSs tend to be discharged with higher power during high electricity purchase price periods (e.g. from 17:00 to 19:00) to reduce the cooling demand for cost savings. In order to gain a higher discharging power, the VESSs tend to be charged with high power before the discharging process to storage enough cooling power for the discharging dispatch. Taking the building B as an example, the discharging power of the VESS reaches its peak (177.823 kW) at 17:30 which is the highest electricity purchase price period (159.04$/MW h). To obtain this high discharging power, the building B based VESS is dispatched to be charged with a high power (177.823 kW) at 17:15 to storage

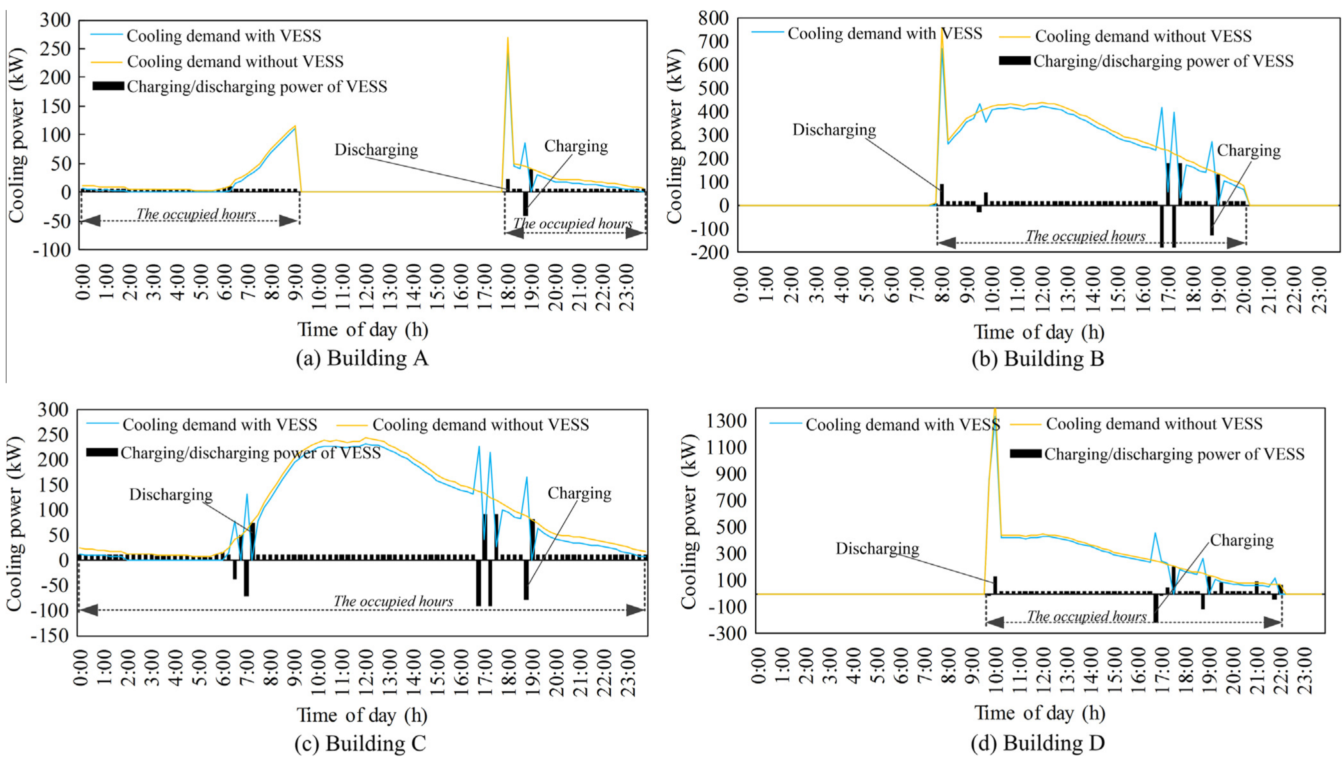

Fig. 12. Dispatch results of the VESSs in a typical day.

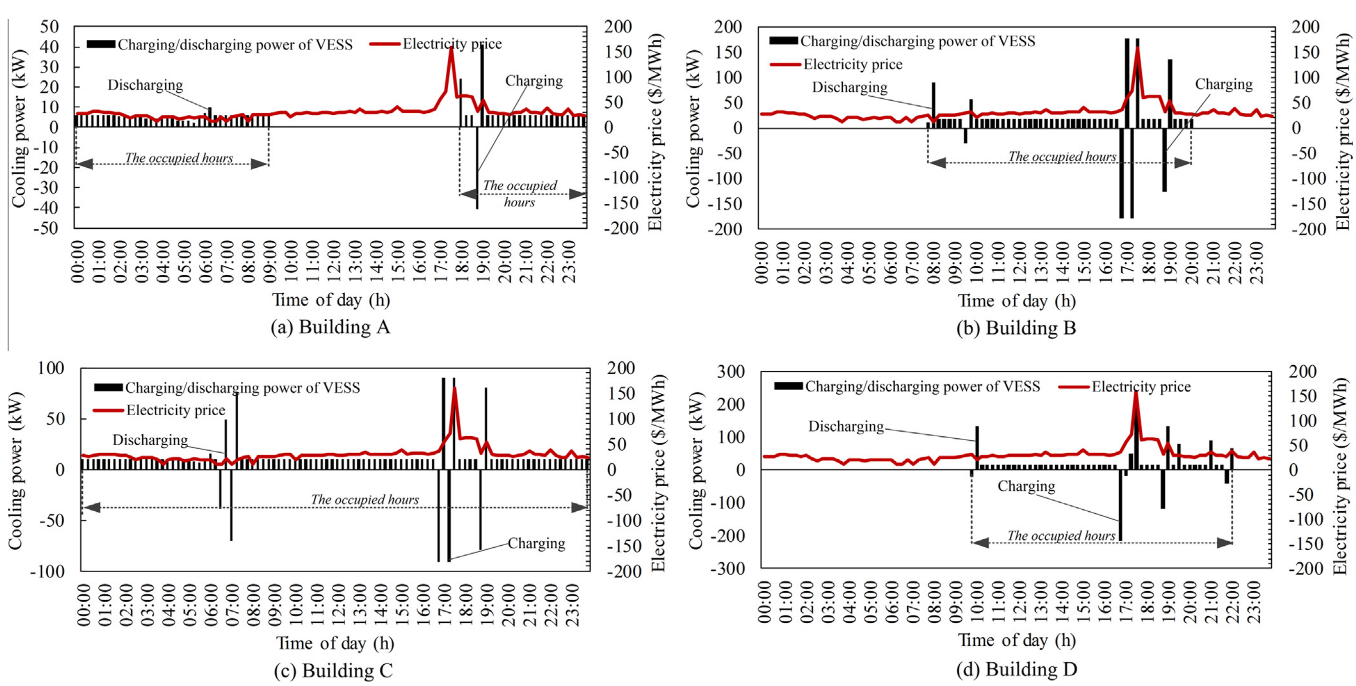

Fig. 13. Relationship between dispatch results of VESSs and electricity prices.

Please cite this article in press as: Jin X et al. Dynamic economic dispatch of a hybrid energy microgrid considering building based virtual energy storage system. Appl Energy (2016), http://dx.doi.org/10.1016/j.apenergy.2016.07.080

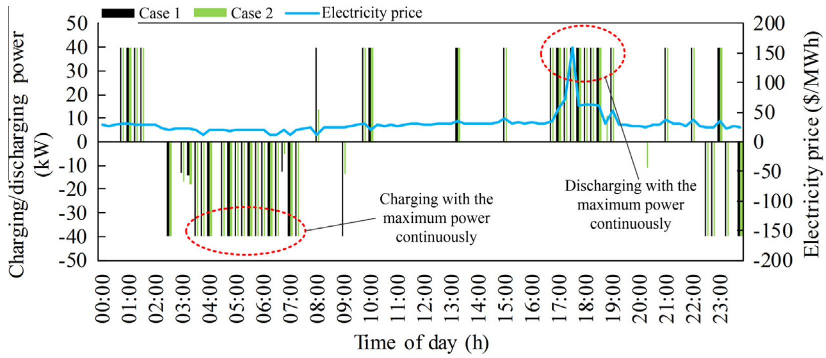

Fig. 14. Dispatch results of the BESS in a typical day.

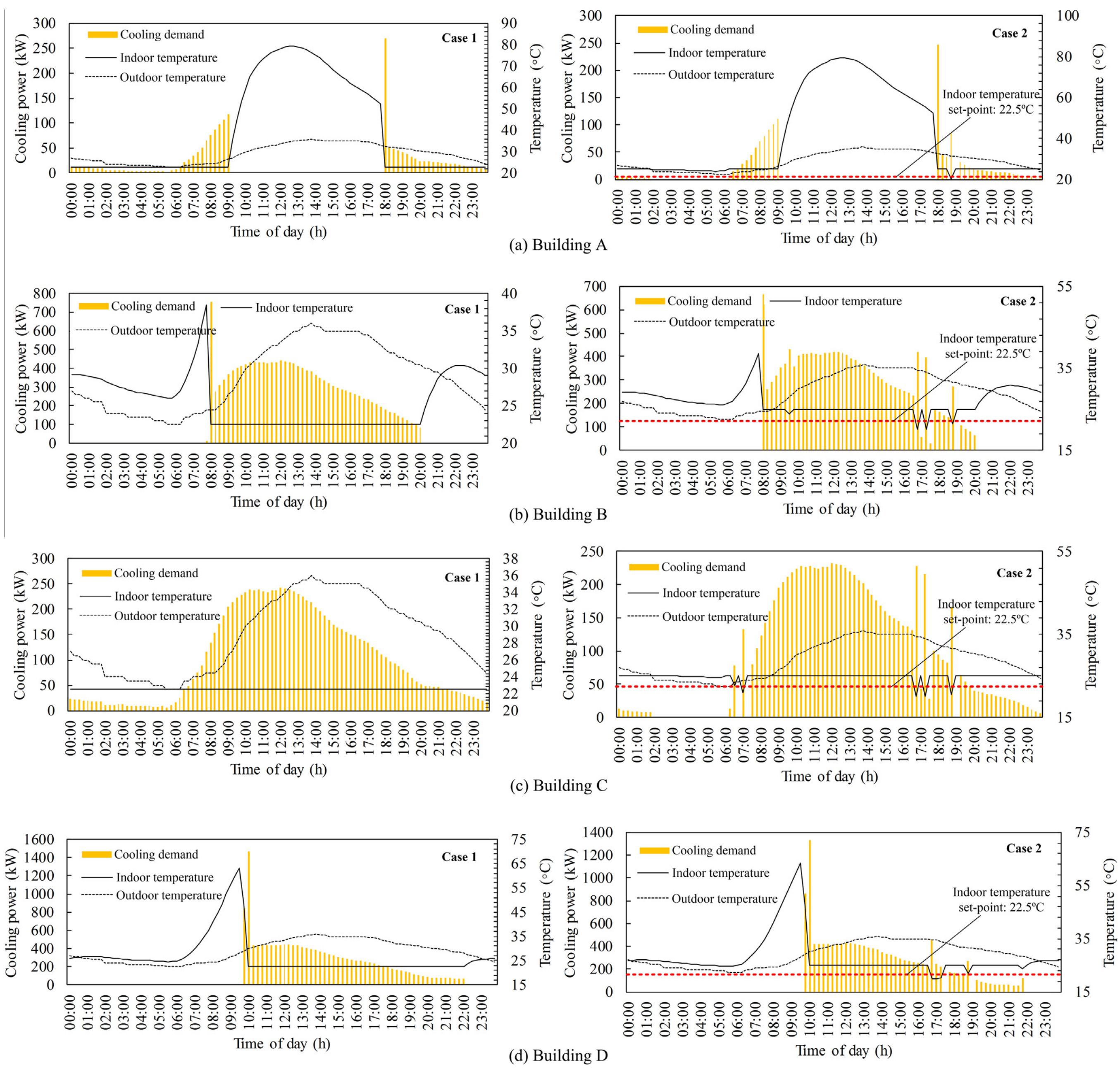

Fig. 15. Dispatch results of the cooling demands with indoor temperatures of the buildings in a typical day.

Please cite this article in press as: Jin X et al. Dynamic economic dispatch of a hybrid energy microgrid considering building based virtual energy storage system. Appl Energy (2016), http://dx.doi.org/10.1016/j.apenergy.2016.07.080

enough cooling energy before the discharging process at 17:30. Consequently, the time-sensitive electricity prices play an important role in the DED of the H-Microgrid considering the VESSs.

The dispatch results of the BESS in a day are shown in Fig. 14. As depicted in Fig. 14, the BESS can be charged with its maximum power continuously during low electricity price and discharged with its maximum power continuously during high electricity price. In contrast, as shown in Fig. 13, although the VESSs can be discharged continuously in several time intervals, the discharging power tends to be lower. Furthermore, before the higher power discharging process, the VESSs are charged with high power to storage enough cooling energy. And after the higher power discharging process, the VESSs are discharged with low power or dispatched to operate in charging mode to satisfy the indoor temperature constraints. The main reason is that the building based VESS has a relatively fast energy dissipation characteristic, while the self-discharge ratio of the BESS is very low [53].

The dispatch results of the building based VESSs are also closely linked to the indoor temperatures of the buildings because the indoor temperatures of the buildings are adjusted within the customer temperature comfort ranges to manage the charging/discharging power of the VESSs. The dispatch results of the cooling demands with indoor temperatures of the buildings in a day are depicted in Fig. 15. We can observe that the indoor temperatures fluctuate around the indoor temperature set-point (22.5 °C) within the indoor temperature comfort range (20–25 °C) during the occupied hours in Case 2, while the indoor temperatures keep at the set-points during the occupied hours in Case 1. Thanks to the indoor temperatures adjustments of the buildings, the VESSs are managed to participate in the DED of the H-Microgrid to reduce the daily operating cost and the customer temperature comfort levels are guaranteed at the same time.

5. Conclusion

A DED model of a H-Microgrid considering building based VESS was proposed in this paper. Firstly, the mathematical relationship among the indoor temperature, cooling demand and outdoor temperature was established in this paper based on the building thermal equilibrium equation. Then, a building based VESS model was developed as a dispatchable unit to participate in the DED of the H-Microgrid for daily operating cost reduction.

The heat transfer through the external walls, the heat transfer across the windows, internal heat gains, the heat contribution due to the solar radiation on the opaque surface of the external walls at different wall orientations, the whole solar radiation transmitted across the windows at different wall orientations and the cooling power generated by the cooling equipment were considered in the VESS model.

Based on the developed VESS model, a DED model for daily operating cost reduction was proposed. The proposed DED method can make full use of the available capacity of the VESSs to reduce the daily operating cost, and guarantee the customer temperature comfort level at the same time. The DED of the H-Microgrid with VESS has benefits in daily operating cost reduction, less startup and shutdown times of the dispatchable DGs and more free capacity of the dispatchable DGs.

Numerical studies show that the dispatch results of the VESSs are closely related to the occupied hours of the buildings, the parameters of the buildings and the time-sensitive electricity prices. Due to the different occupied hours and different parameters of the four buildings investigated as case studies, the four building based VESSs are dispatched during different time periods and present different charging/discharging characteristics. The dispatch results of the VESS change in accordance with the fluctuation of the electricity prices: The VESS tends to be discharged with higher power during high electricity purchase price periods and be charged with higher power before the discharging process for daily operating cost reduction. Also, the VESS and the BESS present different charging/discharging characteristics, because the VESS has a relatively fast energy dissipation characteristic, while the self-discharge ratio of the BESS is very low.

Acknowledgements

This work was financially supported by the National High-tech R&D Program of China (863 Program with No. 2015AA050403), the project National Natural Science Foundation of China (Grant Nos. 51307115, 51377117, and 51277128), and Tianjin Municipal Science and Technology Development Program of China (Grant No. 15JCQNJC43500).

References

[1] Keirstead J, Jennings M, Sivakumar A. A review of urban energy system models: approaches, challenges and opportunities. Renew Sustain Energ Rev 2012;16(6):3847–66.
[2] Guan X, Xu Z, Jia QS. Energy-efficient buildings facilitated by microgrid. IEEE Trans Smart Grid 2010;1(1):243–52.
[3] International Energy Agency. Energy technology perspectives 2012: pathways to a clean energy system. Paris (France): International Energy Agency; 2012.
[4] The European Parliament. Directive 2010/31/EU of the European Parliament and the Council on 19 May 2010 on the energy performance of buildings (recast). Off. J. Eur. Union 2010;153(June):13–35.
[5] Efficient building advocates, meet China. The Institute for Building Efficiency. http://www.institutebe.com/energy-policy/efficiency-building-advocates-meet-china.aspx.
[6] Yu J, Tian L, Xu X, et al. Evaluation on energy and thermal performance for office building envelope in different climate zones of China. Energy Build 2015;86:626–39.
[7] Amecke H, Deason J, Hobbs A, et al. Buildings energy efficiency in China, Germany, and the United States. Climate Policy Initiative; 2013.
[8] Bin S, Jun L. Building energy efficiency policies in China: Status report. Global Buildings Performance Network; 2012.
[9] Diamond RC, Ye Q, Feng W, et al. Sustainable building in China—a green leap forward. Buildings 2013;3(3):639–58.
[10] Xu X, Jia H, Wang D, et al. Hierarchical energy management system for multi-source multi-product microgrids. Renew Energy 2015;78:621–30.
[11] Xu X, Jin X, Jia H, et al. Hierarchical management for integrated community energy systems. Appl Energy 2015;160:231–43.
[12] Zhao Y, Lu Y, Yan C, et al. MPC-based optimal scheduling of grid-connected low energy buildings with thermal energy storages. Energy Build 2014;86:415–26.
[13] Lu Y, Wang S, Sun Y, Yan C. Optimal scheduling of buildings with energy generation and thermal energy storage under dynamic electricity pricing using mixed-integer nonlinear programming. Appl Energy 2015;147:49–58.
[14] Jaramillo LB, Weidlich A. Optimal microgrid scheduling with peak load reduction involving an electrolyzer and flexible loads. Appl Energy 2016;169:857–65.
[15] Jia H, Qi Y, Mu Y. Frequency response of autonomous microgrid based on family-friendly controllable loads. Sci China Technol Sci 2013;56:693–702.
[16] Mu Y, Wu J, Ekanayake J, Jenkins N, Jia H. Primary frequency response from electric vehicles in the Great Britain power system. IEEE Trans Smart Grid 2013;4(2):1142–50.
[17] Mu Y, Wu J, Jenkins N, et al. A spatial–temporal model for grid impact analysis of plug-in electric vehicles. Appl Energy 2014;114:456–65.
[18] Van Roy J, Leemput N, Geth F, et al. Electric vehicle charging in an office building microgrid with distributed energy resources. IEEE Trans Sustain Energy 2014;5(4):1–8.
[19] Liu N, Chen Q, Liu J, et al. A heuristic operation strategy for commercial building micro-grids containing EVs and PV system. IEEE Trans Ind Electron 2014;62(4):2560–70.
[20] Igualada L, Corchero C, Cruz-Zambrano M, et al. Optimal energy management for a residential microgrid including a vehicle-to-grid system. IEEE Trans Smart Grid 2014;5(4):2163–72.
[21] Rabiee A, Sadeghi M, Aghaeic J, et al. Optimal operation of microgrids through simultaneous scheduling of electrical vehicles and responsive loads considering wind and PV units uncertainties. Renew Sustain Energ Rev 2016;57:721–39.
[22] Bahmani-Firouzi B, Farjah E, Seifi A. A new algorithm for combined heat and power dynamic economic dispatch considering valve-point effects. Energy 2013;52:320–32.
[23] Wu H, Liu X, Ding M. Dynamic economic dispatch of a microgrid: mathematical models and solution algorithm. Int J Elect Power Energy Syst 2014;63:336–46.

Please cite this article in press as: Jin X et al. Dynamic economic dispatch of a hybrid energy microgrid considering building based virtual energy storage system. Appl Energy (2016), http://dx.doi.org/10.1016/j.apenergy.2016.07.080

[24] Zaman MF, Elsayed SM, Ray T, et al. Evolutionary algorithms for dynamic economic dispatch problems. IEEE Trans Power Syst 2016;31(2):1486–95.
[25] Yang L, Li Y. Cooling load reduction by using thermal mass and night ventilation. Energy Build 2008;40(11):2052–8.
[26] Cristofari C, Norvaišienė R, Canaletti JL, Nottona G. Innovative alternative solar thermal solutions for housing in conservation-area sites listed as national heritage assets. Energy Build 2015;89:123–31.
[27] Rosa MD, Bianco V, Scarpa F, et al. Heating and cooling building energy demand evaluation; a simplified model and a modified degree days approach. Appl Energy 2014;128(3):217–29.
[28] Yang IH, Yeo MS, Kim KW. Application of artificial neural network to predict the optimal start time for heating system in building. Energy Convers Manage 2003;44(17):2791–809.
[29] ISO 13790:2008. Energy performance of buildings-calculation of energy use for space heating and cooling; 2008.
[30] ISO 6946:2007. Building components and building elements-thermal resistance and thermal transmittance-calculation method; 2007.
[31] Ozel M, Pihtili K. Optimum location and distribution of insulation layers on building walls with various orientations. Build Environ 2007;42(8):3051–9.
[32] Duffie JA, Beckman WA. Solar engineering of thermal process. New York: Wiley; 1991.
[33] Zainal OA, Yumrutaş R. Validation of periodic solution for computing CLTD (cooling load temperature difference) values for building walls and flat roofs. Energy 2015;82:758–68.
[34] IBM ILOG CPLEX optimization solver 12.2.
[35] Zhang N, Kang C, Xia Q, et al. A convex model of risk-based unit commitment for day-ahead market clearing considering wind power uncertainty. IEEE Trans Power Syst 2014;30(3):1582–92.
[36] Su W, Wang J, Zhang K, et al. Model predictive control-based power dispatch for distribution system considering plug-in electric vehicle uncertainty. Elect Power Syst Res 2014;106(1):29–35.
[37] Buonomano A, Palombo A. Building energy performance analysis by an in-house developed dynamic simulation code: an investigation for different case studies. Appl Energy 2014;113(6):788–807.
[38] Best RE, Flager F, Lepech MD, et al. Modeling and optimization of building mix and energy supply technology for urban districts. Appl Energy 2015;159:161–77.
[39] Marino C, Minichiello F, Bahnfleth W. The influence of surface finishes on the energy demand of HVAC systems for existing buildings. Energy Build 2015;95:70–9.
[40] Kaşka Önder, Yumrutaş R. Experimental investigation for total equivalent temperature difference (TETD) values of building walls and flat roofs. Energy Convers Manage 2009;50(11):2818–25.
[41] Hazyuk I, Ghiaus C, Penhouet D. Optimal temperature control of intermittently heated buildings using model predictive control: Part I – building modeling. Build Environ 2011;51(7):379–87.
[42] Magyar Z, Garbai L, Jasper A. Risk-based determination of heat demand for central and district heating by a probability theory approach. Energy Build 2016;110:387–95.
[43] Mui KW. Energy policy for integrating the building environmental performance model of an air conditioned building in a subtropical climate. Energy Convers Manage 2006;47(15–16):2059–69.
[44] Haniff MF, Selamat H, Yusof R, et al. Review of HVAC scheduling techniques for buildings towards energy-efficient and cost-effective operations. Renew Sustain Energ Rev 2013;27(8):94–103.
[45] New York independent system operator; August, 2015. [Online]. Available: http://www.nyiso.com.
[46] Wu X, Wang X, Qu C. A hierarchical framework for generation scheduling of microgrid. IEEE Trans Power Delivery 2014;29(6):2448–57.
[47] Li P, Xu D, Zhou Z, et al. Stochastic optimal operation of microgrid based on chaotic binary particle swarm optimization. IEEE Trans Smart Grid 2016;7(1):66–73.
[48] Chen SX, Gooi HB, Wang MQ. Sizing of energy storage for microgrids. IEEE Trans Smart Grid 2012;3(1):142–51.
[49] Jabbari-Sabet R, Moghaddas-Tafreshi SM, Mirhoseini SS. Microgrid operation and management using probabilistic reconfiguration and unit commitment. Int J Elect Power Energy Syst 2016;75:328–36.
[50] Alharbi W, Raahemifar K. Probabilistic coordination of microgrid energy resources operation considering uncertainties. Elect Power Syst Res 2015;128:1–10.
[51] Basu AK. Microgrids: planning of fuel energy management by strategic deployment of CHP-based DERs – an evolutionary algorithm approach. Int J Elect Power Energy Syst 2013;44(1):326–36.
[52] Kelouwani S, Adegnon K, Agbossou K, et al. Online system identification and adaptive control for PEM fuel cell maximum efficiency tracking. IEEE Trans Energy Convers 2012;27(3):580–92.
[53] Loukarakis E, Dent CJ, Bialek JW. Decentralized multi-period economic dispatch for real-time flexible demand management. IEEE Trans Power Syst 2016;31(1):672–84.

Please cite this article in press as: Jin X et al. Dynamic economic dispatch of a hybrid energy microgrid considering building based virtual energy storage system. Appl Energy (2016), http://dx.doi.org/10.1016/j.apenergy.2016.07.080